2017 International Nuclear Atlantic Conference - INAC 2017
Belo Horizonte, MG, Brazil, October 22-27, 2017
ASSOCIAÇÃO BRASILEIRA DE ENERGIA NUCLEAR – ABEN

EVALUATION OF ITERATIVE ALGORITHMS FOR TOMOGRAHY IMAGE RECONSTRUCTION – A STUDY USING A THIRD GENERATION INSDUTRIAL TOMOGRAPHY SYSTEM

Alexandre F. Velo[1], Diego V. Carvalho[1], Alexandre G. Alvarez, Margarida M. Hamada[1] and Carlos H. Mesquita[1]

[1] Instituto de Pesquisas Energéticas e Nucleares (IPEN / CNEN - SP)
Av. Professor Lineu Prestes 2242
05508-000 São Paulo, SP
afvelo@usp.br

ABSTRACT

The greatest impact of the tomography technology currently occurs in medicine. The success is due to the human body presents standardized dimensions with well-established composition. These conditions are not found in industrial objects. In industry, there is much interest in using the tomography in order to know the inner of (i) the manufactured industrial objects or (ii) the machines and their means of production. In these cases, the purpose of the tomography is to (a) control the quality of the final product and (b) to optimize production, contributing to the pilot phase of the projects and analyzing the quality of the means of production. This scan system is a non-destructive, efficient and fast method for providing sectional images of industrial objects and is able to show the dynamic processes and the dispersion of the materials structures within these objects. In this context, it is important that the reconstructed image presents a great spatial resolution with a satisfactory temporal resolution. Thus the algorithm to reconstruct the images has to meet these requirements. This work consists in the analysis of three different iterative algorithm methods, such Maximum Likelihood Estimation Method (MLEM), Maximum Likelihood Transmitted Method (MLTR) and Simultaneous Iterative Reconstruction Method (SIRT. The analysis consists on measurement of the contrast to noise ratio (CNR), the root mean square error (RMSE) and the Modulation Transfer Function (MTF), to know which algorithm fits better the conditions in order to optimize system. The algorithms and the image quality analysis were performed by the Matlab® 2013b.

1. INTRODUCTION

Unlike the standard aspect of the computed tomography (CT) for medical application, tomography systems for the industrial applications should be adapted to the different size and geometry objects usually placed in an aggressive environment, which contains flammable superheated or corrosive materials, and may be, eventually, subject to high internal pressure: all these factors bring in many difficulties for setting CT devices around the objects [1,2]. Therefore, the development of special CTs is required, inhibiting its production in large scale. In addition, the industrial systems involve dynamic processes and contain solids, liquids and gases mixtures when CT is an excellent option to see the phases distribution inside the vessels [3,4,5,6,7]. In other words, it is necessary to develop a tomographic system suitable for each purpose in industry [2, 6].

The CT systems based on transmission use an array of encapsulated radioactive sources and detectors placed in opposite sides of the targeted object. [7,8,9,10]. First generation tomography systems consist of a source emitting a collimated radiation linear beam and a

radiation detector (Fig.2a). The source-detector system moves in opposite sides of the object, measuring the attenuation of radiation at each position.

In the second generation CT systems, a set of detectors is placed opposite to a set of radioactive sources, moving (source and detector) around the object under study (Fig.2b).

In the tomography of third generation, the source is collimated so that the path crossed by beams is similar to a fan (Fig.2c). The system moves around the targeted object, obtaining a particular view for an "x" position of the source-detector array. In this type of system, several sources and arrays of multiple detectors may be used.

Finally, the so-called fourth-generation CT systems use a fixed array of detectors (a large number of detectors mounted on a fixed ring) and a radioactive source that moves around the object (Fig.2d). Records of any measure are from the detector, representing a view of the object. However, all CTs are constituted, basically, of same parts: radioactive sources; radiation detectors; a data acquisition system and a suitable computer.

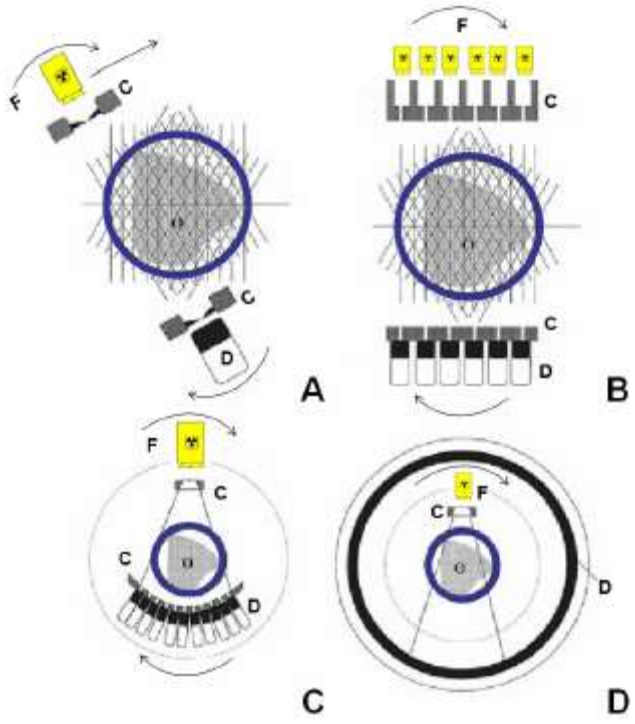

Figure 1: (A) translation - rotation of a beam in parallel (first generation), (B) translation - rotation of multiple sources in parallel (second generation), (C) rotation of a fan-beam (third generation), (D) detector fixed - rotation source (fourth generation). D: detectors; F: source C: collimator, O: object of study

A third generation computed tomography was developed for analysis of industrial multiphase systems at IPEN [2,11]. In its configuration, an array of three NaI(Tl) detectors is located in an arc concentric to the center of the ^{137}Cs gamma source. In order to increase the number of projections measurements in one view of the studied system, the number of detectors in the arc was effectively increased by using a collimator that moves across the detector arc. The whole assembly of the detectors and the radiation source are mounted on a gantry capable of

being rotated round the test section axis through a stepper motor interfaced with a host computer [11].

These scan systems are able to show the dynamic processes and the dispersion of the materials structures within objects. In this context, it is important that the tomography reconstructed image presents a great spatial resolution with a satisfactory temporal resolution [11,12]. Thus the algorithm selected to reconstruct the images has to meet these requirements. The aim of this work consists in the analysis of different iterative algorithms of reconstruction method.

2. MATERIAL AND METHODS

2.1. Image Acquisition

A third generation computed tomography system, comprising three NaI(Tl) detectors of 50 x 50 mm^2 (diameter, thickness) shielded with lead, was used. The detectors were placed on a gantry in fan-beam geometry opposite to the gamma ray source, as shown in Fig.1. The three NaI(Tl) detectors were individually collimated with lead containing a septa of 2 x 5 x 50 mm^3 (width, height, depth). The detectors move 53 times in a step angle of 0.226 degree, emulating 159 detectors per projection. The counting time for sampling was 5 seconds. Thereafter, the support table containing the gantry and the ^{137}Cs gamma source (Fig. 1) rotates six degrees forward, and this process goes on up to completing 360 degrees, totalizing 60 projections. For a total of 9540 samples (159 'virtual detectors' x 60 projections) the system spends 15,900 seconds or 4.4 hours to obtain each tomography image. The ^{137}Cs radioactive source, with an activity of 3.0 GBq (81 mCi), was placed into a radioactive shield-case with an aperture angle of 36 degrees (Fig. 2). This system was previously described by Mesquita et al [12,13].

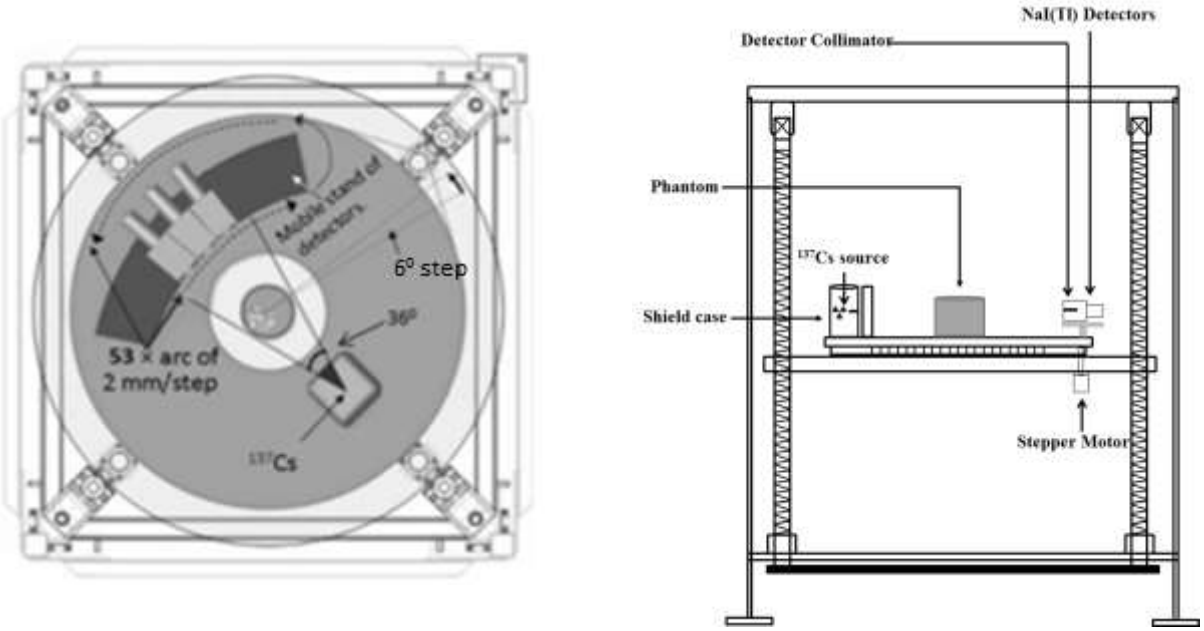

Figure 2: Diagram of the third generation CT scanner used. (a) Top view and (b) side view

2.2. Multiphase Phantom and CT Characterization

A multiphase phantom was used to evaluate the performance of the multisource third generation tomography device [12]. The phantom consists of a polymethylmethacrylate (PMMA (($\rho \approx 1.19$ g/cm^3)) solid cylinder containing three holes: one filled with steel ($\rho \approx 7.874$ g/cm^3), another with aluminum ($\rho \approx 2.698$ g/cm^3) and the third one empty (filled with air) and surrounded with glass, as illustrated in Fig. 3.

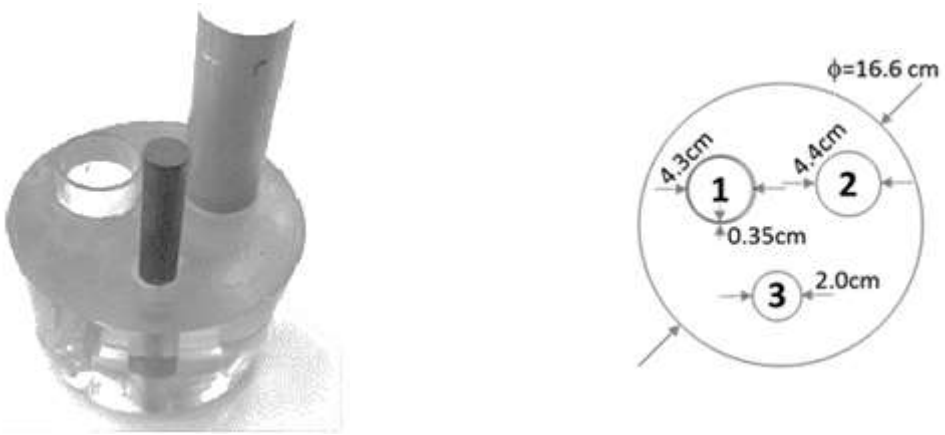

Figure 3: Illustration of the multiphase phantom scheme. 1- Air surrounded with glass wall, 2-aluminum bar and 3-steel bars. The phantom is made of acrylic

2.3. Iterative Algorithms

The image reconstruction is based on the exponential decay law defined by the equation (1), which is known as Lambert-Beer's law [14]:

$$I=I_0 \cdot e^{\sum_{i=1}^{N} \mu_i \cdot w_{i,\vec{j}}} \quad (1)$$

where $\boldsymbol{I_0}$ is the initial intensity of the beam radiation that focuses on the object on $\vec{j}$ direction, $\boldsymbol{I}$ is the intensity of the beam radiation through the object, N is the number of pixels on matrix, $\boldsymbol{\mu_I}$ is the mass attenuation coefficient of the matter on pixel $\boldsymbol{I}$ and $w_{i,\vec{j}}$ is the length of the beam radiation through the pixel on pixel $\boldsymbol{I}$ on$\vec{j}$. $w_{i,\vec{j}}$ is defined as weighted matrix (W) (Fig. 3) element [14].

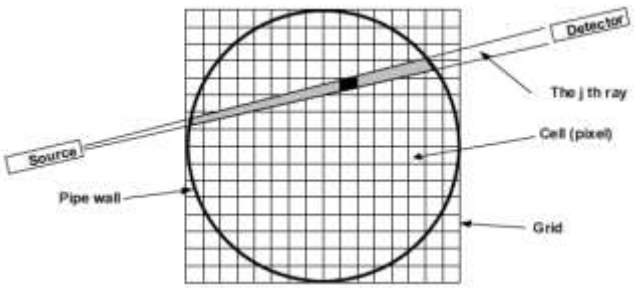

Figure 3: Discretized object [12]

The discretized ray sum for each ray j (j = 1, 2, …, J) can be expressed as the equation (2) [14].

$$p_j^{normalized} = ln\left(\frac{I_{oj}}{I_j}\right) = \sum_{i=1}^{N} w_{ij}\mu_i \tag{2}$$

where N is the number of pixels. The term w_{ji} represents an element of the weight matrix (W), and is defined as the intersectional area between the j^{th} ray and the i^{th} pixel divided by the intersectional area between the j^{th} ray and the sample. The size of W is defined by the number of pixels in the reconstruction grid. Due to Poisson noise corruption of the measured data, a term $\eta_j$describing the noise is added to the equation (3) [14]:

$$p_j^{normalized} = ln\left(\frac{I_{oj}}{I_j}\right) = \sum_{i=1}^{N} w_{ij}x_i + \eta_j \tag{3}$$

Solving a high number of linear equations based on measurements corrupted by random variables and noise, requires the use of iterative algorithms. The iterative methods are divided in two categories, the algebraic and the statistical [14]. Algebraic reconstruction methods solve a set of linear equations by comparing the measured data set to an estimate and reduce the difference between these. Statistical methods reconstruct the image by implementing the maximization of the likelihood function, recognizing the Poisson distribution function of the projections with the measured [14]. In the present work, the Simultaneous Iterative Reconstruction Technique (SIRT), Maximum Likelihood Expectation Maximization (MLEM) and Maximum Likelihood Algorithm for Transmission Tomography (MLTR) were used to reconstruct the images, where the first algorithm is an algebraic method and the last two are statistical methods.

The algebraic method SIRT is expressed by equation (4) [14].

$$f_j^{(n+1)} = f_j^n + \delta \sum_{i=1}^{M} h_{ij} \frac{\left(g_i - \sum_{k=1}^{N} h_{ik} f_k^{(n)}\right)}{\sum_{k=1}^{N} h_{jk}^2} \tag{4}$$

where f is the pixel index, δ is the relaxation parameter, g is the $P_{normalized}$ and h is the weight matrix.

The statistical methods MLTR and MLEM are expressed by equations (5) and (6) respectively [14].

$$f_j^{(n+1)} = f_j^{(n)} + \frac{\sum_{i=1}^{M}\left(h_{ij}\left(I_0 e^{\left(-\sum_{k=1}^{N} h_{ik} f_k^{(n)}\right)} - I\right)\right)}{\sum_{i=1}^{M}\left(h_{ij} I_0 e^{\left(-\sum_{k=1}^{N} h_{ik} f_k^{(n)}\right)} \sum_{k=1}^{N} h_{ik}\right)} \tag{5}$$

$$f_j^{(n+1)} = \frac{\sum_{i=1}^{M}\left[I_0 e^{\left(-\sum_{k=1}^{N} h_{ik} f_k^{(n)}\right)}\left(1 - e^{-h_{ij} f_j^{(n)}}\right)\right]}{\sum_{i=1}^{M}\left[I_i - \overline{I_i} + 0.5(1 + e^{-h_{ij} f_j^{(n)}}) I_0 e^{\left(-\sum_{k=1}^{N} h_{ik} f_k^{(n)}\right)}\right]} \quad (6)$$

All reconstruction was performed in a matrix of 128x128 pixels and 200 iterations. All physical measurements and reconstructions were performed by the Matlab 2013b®.

2.4. Physical Measurements

The Root Mean Square Error (RMSE) was measured to evaluate which algorithm of reconstruction approaches the pixel values that correspond to the linear attenuation coefficient, obtained by the reconstruction, to the theoretical values. This method is widely used to measure the quality of the image. The RMSE was calculated by the equation (7) [15].

$$RMSE = \sqrt{\frac{\sum_{i=1}^{N}(\mu_i - \widehat{\mu_i})^2}{N}} \quad (7)$$

where μ_i is the experimental pixel value obtained, $\widehat{\mu_i}$ is the theoretical linear attenuation coefficient. The theoretical image is presented by the Fig. 4.

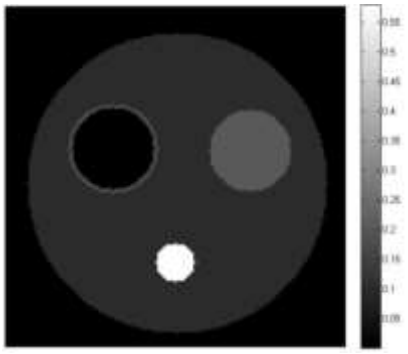

Figure 4: Theoretical image

The Contrast to Noise Ratio (CNR) was measured placing regions of interest (ROIs) in the images obtained by the phantom (Fig. 2) with the different algorithms. A circular ROI was placed over the cylinder corresponding the aluminum (ROI A) and another ROI, with the same size of the ROI A, placed over the background, corresponding the PMMA (ROI B), then the values of the CNR was obtained by the equation (8) [15,16].

$$CNR = \frac{|\overline{\mu_A} - \overline{\mu_B}|}{\sqrt{\frac{\sigma_A^2 + \sigma_B^2}{2}}} \quad (8)$$

where $\overline{\mu_A}$ is the mean pixel value of the ROI A, $\overline{\mu_B}$ is the mean pixel value of the ROI B, $\sigma_A$is the standard deviation of ROI A and σ_B is the standard deviation of the ROI B. The ROIs is represented on Fig. 5, where the red circle represents the ROI A and the blue circle represents the ROI B.

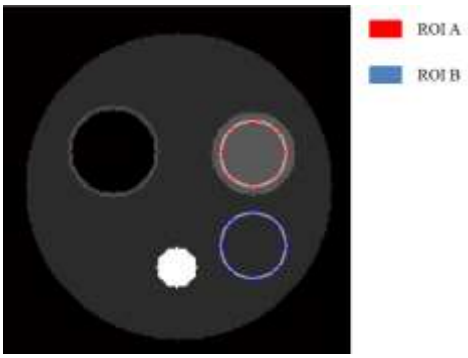

Figure 5: ROIs used to measure the CNR

The most comprehensive metric used to measure and report spatial resolution of imaging systems is the modulation transfer function (MTF) [16,18,19]. Conventionally, the spatial resolution is estimated as the inverse of the value at 10% of MTF curve [16,18,19]. In the present work, MTF was calculated using the Edge Spread Function, commonly known as ESF parameter [18,19].

3. RESULTS AND DISCUSSION

The reconstructed images obtained by the third generation industrial tomography are presented by the Fig. 6, where Fig. 6a. represents the SIRT algorithm; Fig. 6b. the MLTR algorithm; and Fig. 6c. is the MLEM algorithm.

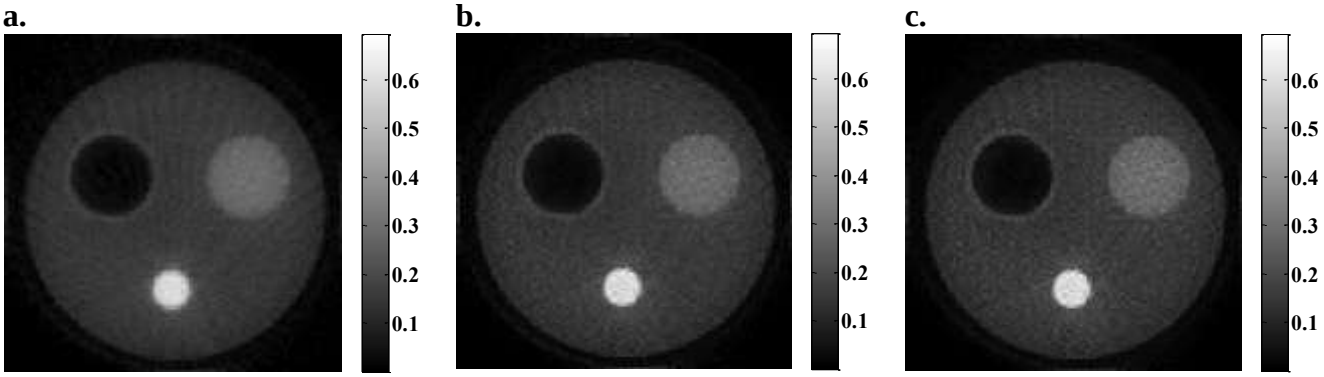

Figure 6: Images reconstructed by the algorithms a. SIRT; b. MLTR and c. MLEM

The RMSE parameter applied to perform the quality of the image for the three different algorithms (SIRT, MLTR and MLEM) was calculated using equation (7), comparing the experimental images with the theoretical image. Fig. 7 shows the curve behavior for each algorithm.

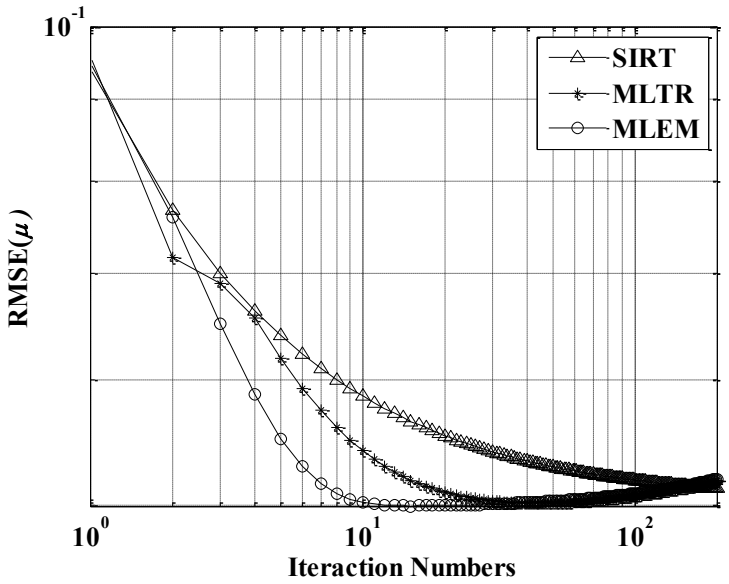

Figure 7: RMSE analysis for the three algorithms

Fig 7 shows that the MLEM algorithm converges and approaches to the theoretical values with less number of iteraction compared to the other two algorithms. This analysis shows that the images reconstructed by the MLEM algorithm has a better quality and converges its optimum with less iteraction number.

The analysis of the noise influence on the quality of the image was performed by the CNR parameter on the three different algorithms. The results are shown by the Fig. 8. By this figure, it is possible to observe that even the MLEM and MLTR algorithm reaches a higher CNR value in the first iteractions, this values decreases rising the number of the iteractions, different of the SIRT algorithm, that reaches a lower CNR value, but decreases less than the others, which means that the noise influence less in the images reconstructed by the SIRT algorithm as the number iteraction increases compared to the other two algorithms.

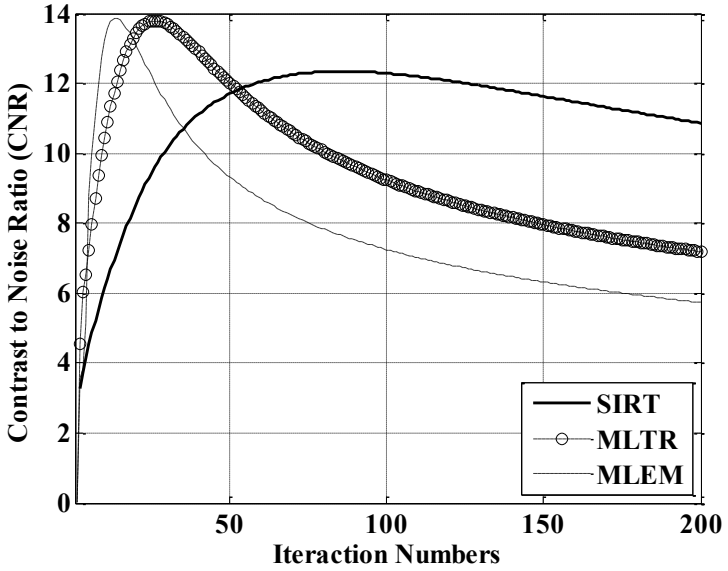

Figure 8: CNR analysis by the number of iteractions

The spatial resolution of the reconstructed images was measured by the MTF (*f*). The MTF curves by the frequency spectrum (plmm^{-1}) of the three algorithms at the iteraction number of 200 are presented by the Fig. 9

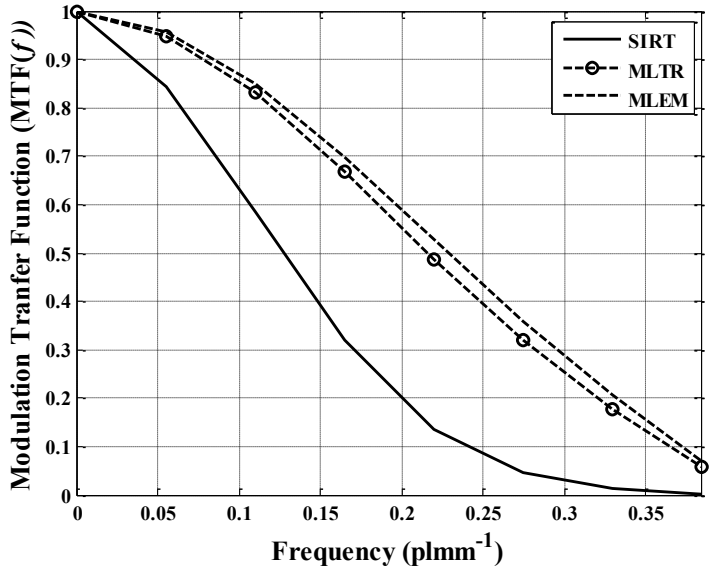

Figure 9: MFT (*f*) of the three different algorithms at the iteractive number of 200

By the Fig. 9, the MLEM algorithm presents a better spatial resolution in all frequency spectrum compared to the others algorithms. The maximum spatial resolution of the system is measured at 10% of the MTF, in other words, the spatial resolution is calculated by the inverse of the frequency in 10% of the MTF. Thereby the resolution for SIRT, MLTR and MLEM is about 2.86 mm, 2.75 mm and 2.70 mm respectively.

Fig. 10 shows the area under the curve of the MTFs obtained for all iteractive number of the three algorithms.

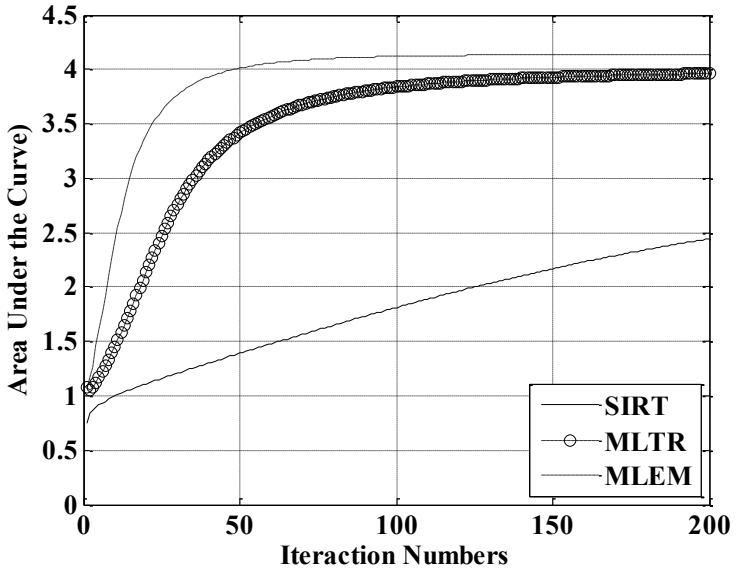

Figure 10: Area under the cure of the MTFs by the number of iteractions

Fig. 10 shows that the MLEM presents a better spatial resolution for all iteractive numbers compared with the others algorithms. It is possible to observe as well, that for the MLEM and the MLTR around 100 iteractions the spatial resolution reaches its optimum value and keeps constant as the iteraction numbers rises. Suggesting that, for these two algorithms, the iteractions could stop at 100, where the spatial resolution reached its higher vale, reducing time of the reconstruction and avoiding the growing of noise as observed on figure 8.

4. CONCLUSIONS

The results of the RMSE values showed that the MLEM algorithm converges and approaches to the theoretical values with less number of iteraction compared to the other two algorithms, evidencing that this algorithm has a better image quality.

The CNR analysis showed that the MLEM and MLTR algorithm reaches a higher CNR value but decreases rising the number of the iteractions due to the growing of the noise, different of the SIRT algorithm, that reaches a lower CNR value, but decreases less than the others, which means that the noise influence less in the images reconstructed by the SIRT algorithm then the other two algorithms.

The spatial resolution value obtained of the SIRT, MLTR and MLEM algorithms is 2.86 mm, 2.75 mm and 2.70 mm respectively, which means that the MLEM has a better spatial resolution.

The area under the curve of the MTFs for all number of iteractions showed that at around 100 iteraction, the spatial resolution for MLTR and MLEM reaches its optimum value, which means that for this two algorithms the iteractions could stop at this value reducing time of

reconstructing and avoiding the growing of noise. The SIRT algorithm has worse spatial resolution, and did not get its optimum value, suggesting that this algorithms has to keep itaraction until reachs the optimum value.
For all the analysis measured, the MLEM is the better algorithm to be applied on the systems of the third generation industrial tomography.

ACKNOWLEDGMENTS

The authors express their acknowledgment to CNEN, FAPESP and IAEA for the financial support. The authors, Carlos Henrique de Mesquita and Margarida Mizue Hamada thank for their fellowship.

REFERENCES

1. KUMAR, S. B.; DUDUKOVIC, M. P., CHAOUKI, J., LARACHI, F., DUDUKOVIC', M. P., *Computer-assisted gamma and X-ray tomography: Application to multiphase flow In Non-Invasive Monitoring of Multiphase Flows*., Eds.; Elsevier: Amsterdam, The Netherlands, 1997; Chapter 2, p 48.
2. MESQUITA, C. H.; VASQUEZ, P. A. S.; HAMADA, M. M. Multi-source third generation computed tomography for industrial multiphase flows applications. *In: 2011 IEEE Nuclear Science Symposium Conference Record*, Oct. 2011 (in press).
3. MESQUITA, C. H.; DANTAS, C.R., COSTA, F.E.; CARVALHO, D.V.S.; MADI, T. F; VASQUEZ, P. A. S.; HAMADA, M. M. Development of a Fourth Generation Industrial Tomography for Multiphase Systems Analysis. In: *2010 IEEE Nuclear Science Symposium Conference Record*, pp. 19-23, Oct. 2010.
4. KUMAR, S. B.; DUDUKOVIC, M. P., Gas holdup in bubble columns at elevated pressure via computed tomography. *Int. J. Multiphase Flows*, **vol. 27**, pp.929-946(2001).
5. ISMAILA; GAMIOG, J. C., Tomography for rmulti-phase flow measurement in the oil industry. *Flow Measurement and Instrumentation*, **vol. 16**, pp. 145-155(2005).
6. VASQUEZ, P. A. S. ; MESQUITA, C. H. ; HAMADA, M. M. . Methodological Analysis of Gamma Tomography System for Large Random Packed Columns. *Applied Radiation and Isotopes***, v. 68**, p. 658-661(2010).
7. IAEA-TECDOC-1589 *Industrial Process Gamma Tomography*, Viena, May 2008
8. VASQUEZ, P. Análise de sistemas multifásicos utilizando tomografia computadorizada gama monoenergética e polienergética. 2008 Tese (Doutorado) –IPEN-USP, São Paulo
9. CHAOUKI, J.; LARACHI, F.; DUDUKOVIC, M. Noninvasive Tomographic and Velocimetric Monitoring of Multiphase Flows. *Ind. Eng. Chem. Res.*, **v. 36**, p. 4476-4503(1997).
10. JOHANSEN, G. A.; JACKSON, P., *Radioisotope Gauges for Industrial Process Measurements*. 2004 John Wiley & Sons, Ltd. ISBN 0-471-48999-9
11. CALVO, W. A. P.; HAMADA, M. M; SPRENGER, F. E.; VASQUEZ, P. A. S.; RELA, P. R.; MARTINS, J. F. T.; PEREIRA, J. C. S. M.; OMI, N. M.; MESQUITA, C. H., Gamma-ray computed tomography Scanners for applications in multiphase system columns. *Nukleonika*; **v. 54(2)**, p. 129-133(2009).
12. C.H. de Mesquita, A.F. Velo, D.V.S. Carvalho, J.F.T. Martins, M.M. Hamada, Industrial tomography using three different gamma ray, *Flow Meas. Instrum.*, **v.47**, p. 1-9(2016).
13. C.H. Mesquita, D.V.S. Carvalho, R. Kirita, P.A.V. Salvador, M.M. Hamada, Gas–liquid distribution in a bubble column using industrial gamma-ray computed tomography. *Rad. Phys. and Chem*. **v. 95**, p. 396-400(2014).
14. MAAD R., Design Optimization of High Speed Gamma-Ray Tomography. A dissertation submitted in partial fulfilment of the requirements for the degree of Doctor of Philosophy in Physics. Department of Physics and Technology University of Bergen Norway, 2009.
15. Velo A.F, Hamada M.M., Carvalho D.V.S., Martins J.F.T, Mesquita C.H., A portable tomography system with seventy detectors and five gamma-ray sources in fan beam geometry simulated by Monte Carlo method. *Flow Meas. Instr*. **v. 53**, p. 89-94(2017).
16. SMITH, STEVEN W. *The scientist and Engineer's Guide to Digital Signal Processing*. 1997
17. CHRISTIANSON O., CHEN, J. J.S., SAIPRASAD G., FILLIBEN, J.J, PESKIN A., TRIMBLE, C.,

SEIGEL, E L., SAMEI, E., An improved index of image quality for task-based performance of CT iterative reconstruction across three commercial implementations. *Radiology*, v**. 275,** p. 725-734(2015).

18. RICHARD S.L, HUSARIK D.B., YADAVA G., MURPHY S.N., SAMEI E. Towards task-based assessment of CT performance: System and object MTF across different reconstruction algorithms. *Med. Phys*, v. 39, p. 4115 – 4122(2012).
19. SAMEI E., FLYNN M.J. and REIMANN D.A. A method for measuring the presampled MTF of digital radiographic systems using an edge test device. *Med. Phys*, **v. 25(1)**, p. 102–113(1998).